JACC: BASIC TO TRANSLATIONAL SCIENCE
VOL. 1, NO. 5, 2016
ISSN 2452-302X
http://dx.doi.org/10.1016/j.jacbts.2016.06.005

PRE-CLINICAL RESEARCH

A Cell-Enriched Engineered Myocardial Graft Limits Infarct Size and Improves Cardiac Function

Pre-Clinical Study in the Porcine Myocardial Infarction Model

Isaac Perea-Gil, MS,[a] Cristina Prat-Vidal, PhD,[a] Carolina Gálvez-Montón, DVM, PhD,[a] Santiago Roura, PhD,[a,b] Aida Llucià-Valldeperas, PhD,[a] Carolina Soler-Botija, PhD,[a] Oriol Iborra-Egea, MS,[a] Idoia Díaz-Güemes, DVM, PhD,[c] Verónica Crisóstomo, DVM, PhD,[c] Francisco M. Sánchez-Margallo, DVM, PhD,[c] Antoni Bayes-Genis, MD, PhD[a,d,e]

VISUAL ABSTRACT

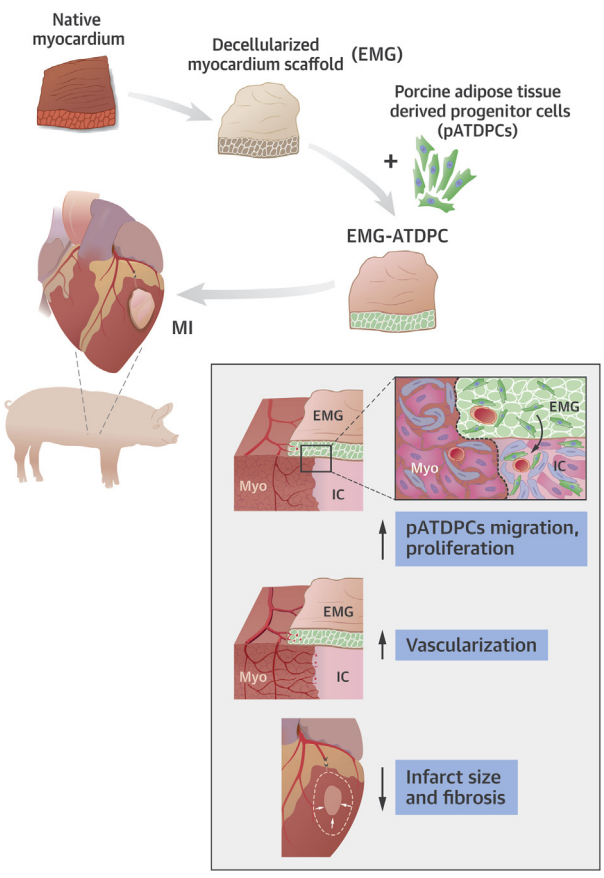

Perea-Gil, I. et al. J Am Coll Cardiol Basic Trans Science. 2016;1(5):360–72.

HIGHLIGHTS

- **MI remains a major cause of morbidity and mortality despite major treatment advances achieved during the past decades.**
- **Administration of an engineered myocardial graft, composed of decellularized myocardial matrix refilled with ATDPCs (EMG-ATDPC), in a porcine pre-clinical MI model, may support cardiac recovery following MI.**
- **Thirty days post-EMG-ATDPC implantation, cardiac magnetic resonance imaging and comprehensive histological analysis were performed to evaluate its impact on myocardial restoration.**
- **EMG-ATDPC resulted in better left ventricular ejection fraction, higher vessel density and neovascularization, and reduced infarct size by 68%, as well as limited fibrosis.**
- **Accordingly, EMG-ATDPC is ready to start the translational avenue toward phase I first-in-man clinical trials.**

From the [a]ICREC (Heart Failure and Cardiac Regeneration) Research Program, Health Science Research Institute Germans Trias i Pujol (IGTP), Badalona, Spain; [b]Center of Regenerative Medicine in Barcelona, Barcelona, Spain; [c]Jesús Usón Minimally Invasive Surgery Centre, JUMISC, Cáceres, Spain; [d]Cardiology Service, Germans Trias i Pujol University Hospital, Badalona, Spain; and the [e]Department of Medicine, Autonomous University of Barcelona (UAB) Barcelona, Spain. This work was supported by grants from

SUMMARY

Myocardial infarction (MI) remains a dreadful disease around the world, causing irreversible sequelae that shorten life expectancy and reduce quality of life despite current treatment. Here, the authors engineered a cell-enriched myocardial graft, composed of a decellularized myocardial matrix refilled with adipose tissue-derived progenitor cells (EMG-ATDPC). Once applied over the infarcted area in the swine MI model, the EMG-ATDPC improved cardiac function, reduced infarct size, attenuated fibrosis progression, and promoted neovascularization of the ischemic myocardium. The beneficial effects exerted by the EMG-ATDPC and the absence of identified adverse side effects should facilitate its clinical translation as a novel MI therapy in humans. (J Am Coll Cardiol Basic Trans Science 2016;1:360–72)

ABBREVIATIONS AND ACRONYMS

ATDPC = adipose tissue-derived progenitor cells

CMR = cardiac magnetic resonance imaging

cTnI = cardiac troponin I

EMG = engineered myocardial graft

GFP = green fluorescent protein

IsoB4 = isolectin B4

LV = left ventricle/ventricular

LVEF = left ventricular ejection fraction

MI = myocardial infarction

pATDPC = porcine adipose tissue-derived progenitor cell

SMA = smooth muscle actin

Cardiovascular disease is the foremost cause of death worldwide, accounting for almost 30% of all deaths and exceeding other growing pandemics, such as diabetes mellitus, cancer, and respiratory infections (1). Myocardial infarction (MI) leads to massive cardiomyocyte loss, collagen scar formation, and ultimately, maladaptive adverse ventricular remodeling (2). Cardiac homeostasis self-regeneration is insufficient following MI injury (3,4). Hence, alternative therapies—including cell and gene therapy and tissue engineering—are being investigated as a means of overcoming current therapeutic limitations and challenges.

SEE PAGE 373

Cardiac tissue engineering uses natural or synthetic support platforms generating functional grafts that can be tightly implanted over injured myocardium (5,6). For optimal cell seeding, the supporting material or scaffold should provide a biomimetic niche resembling the physiological microenvironment, supplying the necessary cues to direct cell differentiation and proliferation, and favoring electromechanical coupling with host tissue (7,8). Decellularized myocardial extracellular matrix meets these requirements because it preserves the native myocardium ultrastructure, mechanical properties, and local matrix milieu (9–12). A recent study reports a refined protocol for obtaining an optimal myocardial scaffold for recellularization (9). Despite the favorable qualities of decellularized myocardial scaffolds, few studies have investigated their use in pre-clinical MI animal models. To date, only 1 report describes administration of a decellularized myocardial scaffold in swine, and it was a cell-free scaffold (13).

In our present study, we applied in a swine acute MI model a novel engineered myocardial graft (EMG) obtained by decellularization of porcine myocardial tissue. Decellularized myocardial scaffolds were left acellular (EMG-cell free) or were repopulated with green fluorescent protein (GFP)-labeled porcine adipose tissue-derived progenitor cells (GFP^+ pATDPCs) to generate cell-enriched grafts (EMG-ATDPC). Both engineered grafts (EMG-cell free and EMG-ATDPC) were applied over infarcted myocardium in allogeneic wild-type swine to assess cardiac function and modulation of scar healing.

METHODS

GENERATION OF EMGs. Myocardial decellularization was performed as previously described (**Figure 1**) (9). Briefly, porcine myocardial tissue slices of ~25 × 25 × 3 mm were initially treated for 72 h with 1% sodium dodecyl sulfate (Sigma-Aldrich, St. Louis, Missouri), followed by a 48-h treatment with Triton X-100 (Sigma-Aldrich). Both solutions were replaced every

the Ministerio de Ciencia e Innovación [SAF2014-59892-R]; Red de Terapia Celular-TerCel (RD12/0019/0029), Red de Investigación Cardiovascular-RIC (RD12/0042/0047) and Fondo de Investigación Sanitaria, Instituto de Salud Carlos III (FIS PI14/01682) projects as part of the Plan Nacional de I+D+I and cofunded by ISCIII-Sudirección General de Evaluación y el Fondo Europeo de Desarrollo Regional (FEDER); Fundació La Marató de TV3 [201502; 201516]; Beca de Recerca Bàsica de l'Acadèmia de Ciències Mèdiques i de la Salut de Catalunya i de Balears 2015; Beca d'Investigació Bàsica de la Societat Catalana de Cardiologia 2015; Generalitat de Catalunya (SGR 2014); and Sociedad Española de Cardiología. The authors also appreciate support from the Fundació Privada Daniel Bravo Andreu. The authors have reported that they have no relationships relevant to the contents of this paper to disclose. Drs. Perea-Gil, Prat-Vidal, and Gálvez-Montón contributed equally to this work.

Manuscript received April 11, 2016; revised manuscript received June 16, 2016, accepted June 16, 2016.

FIGURE 1 Development of EMG-ATDPC and Experimental Design of the in Vivo Study

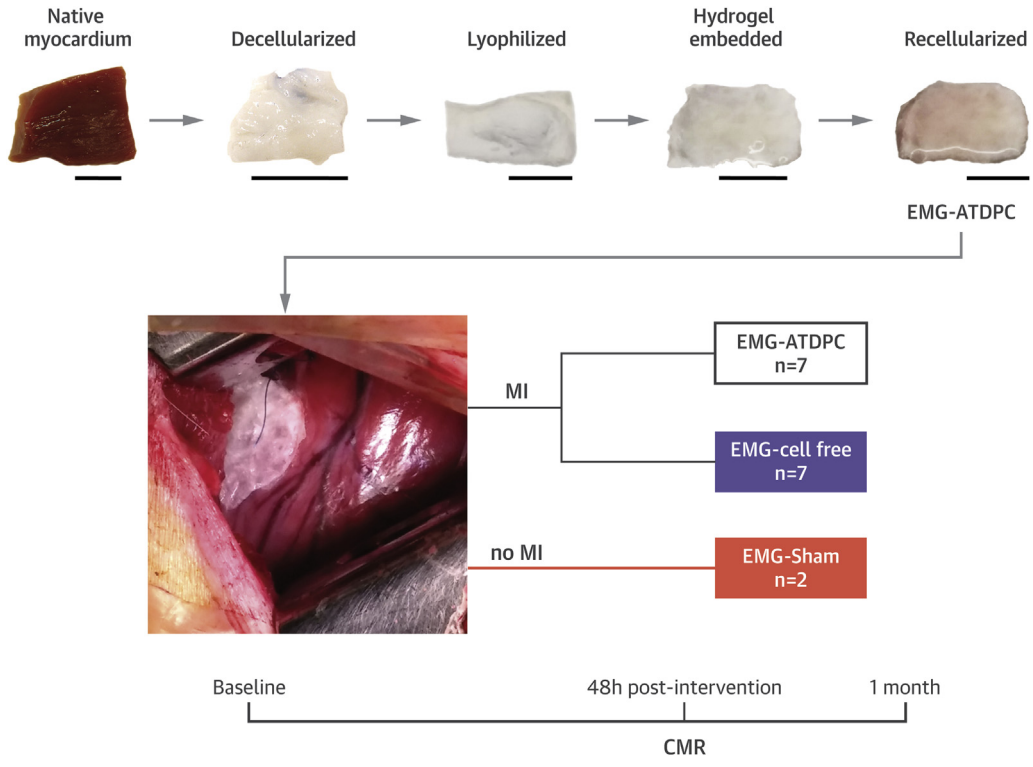

Main steps involved in EMG-ATDPC obtaining from porcine myocardial tissue are shown. n indicates number of pigs. CMR = cardiac magnetic resonance imaging; EMG-ATDPC = engineered myocardial graft repopulated with porcine adipose tissue-derived progenitor cells (pATDPC); MI = myocardial infarction. Scale bars = 1 cm.

24 h. Next, the myocardial tissue was exhaustively washed with phosphate-buffered saline containing 1% penicillin/streptomycin (Gibco, Grand Island, New York), 3 times for 24 h each. All of these steps were repeated twice, and the tissue was washed with sterile distilled water between cycles. Following completion of the second cycle, a 72-h DNase I (Roche, Basel, Switzerland) digestion was performed. The obtained decellularized myocardial scaffolds were next lyophilized in a freeze-drier chamber (Christ loc-1 m, B. Braun Biotech International, Melsungen, Germany), sterilized with a certified gamma irradiation dosage of 30 kGy (Aragogamma, Barcelona, Spain), and stored at room temperature until use.

The EMG-ATDPC was generated by rehydrating the decellularized myocardial scaffold using a mixture of 175 μl of peptide hydrogel RAD16-I (Corning, Corning, New York) and 175 μl of 1.75×10^6 GFP^+ pATDPCs in 10% sucrose (Sigma-Aldrich) (Figure 2A). pATDPCs used were isolated and cultured from pericardial adipose tissue as previously described (14). To obtain the EMG-cell free, the decellularized myocardial scaffold was only rehydrated with 350 μl of RAD16-I hydrogel. Fifteen minutes later, 350 μl of α-MEM (Sigma-Aldrich) was added to the EMG (Figure 2B), and constructs (EMG-ATDPC or EMG-cell free) were implanted in the infarcted area.

EXPERIMENTAL DESIGN. All study procedures followed the guidelines regarding the use of animals in research as established in the Guide for the Care and Use of Laboratory Animals (NIH Publication No. 80-23, revised 1996), and conformed to the principles outlined in the Declaration of Helsinki. The study was approved by the local Animal Experimentation Unit Ethical Committee (Number: ES 100370001499).

A total of 16 crossbred Landrace × Large White pigs (39.0 ± 3.7 kg) were randomly distributed in the following 3 groups:

1. EMG-cell free (n = 8), with MI induction and EMG-cell free implantation;
2. EMG-ATDPC (n = 10), with MI induction and EMG-ATDPC treatment; and

FIGURE 2 **EMG-ATDPC Preparation and Implantation, and Post-MI Morphometric Analysis**

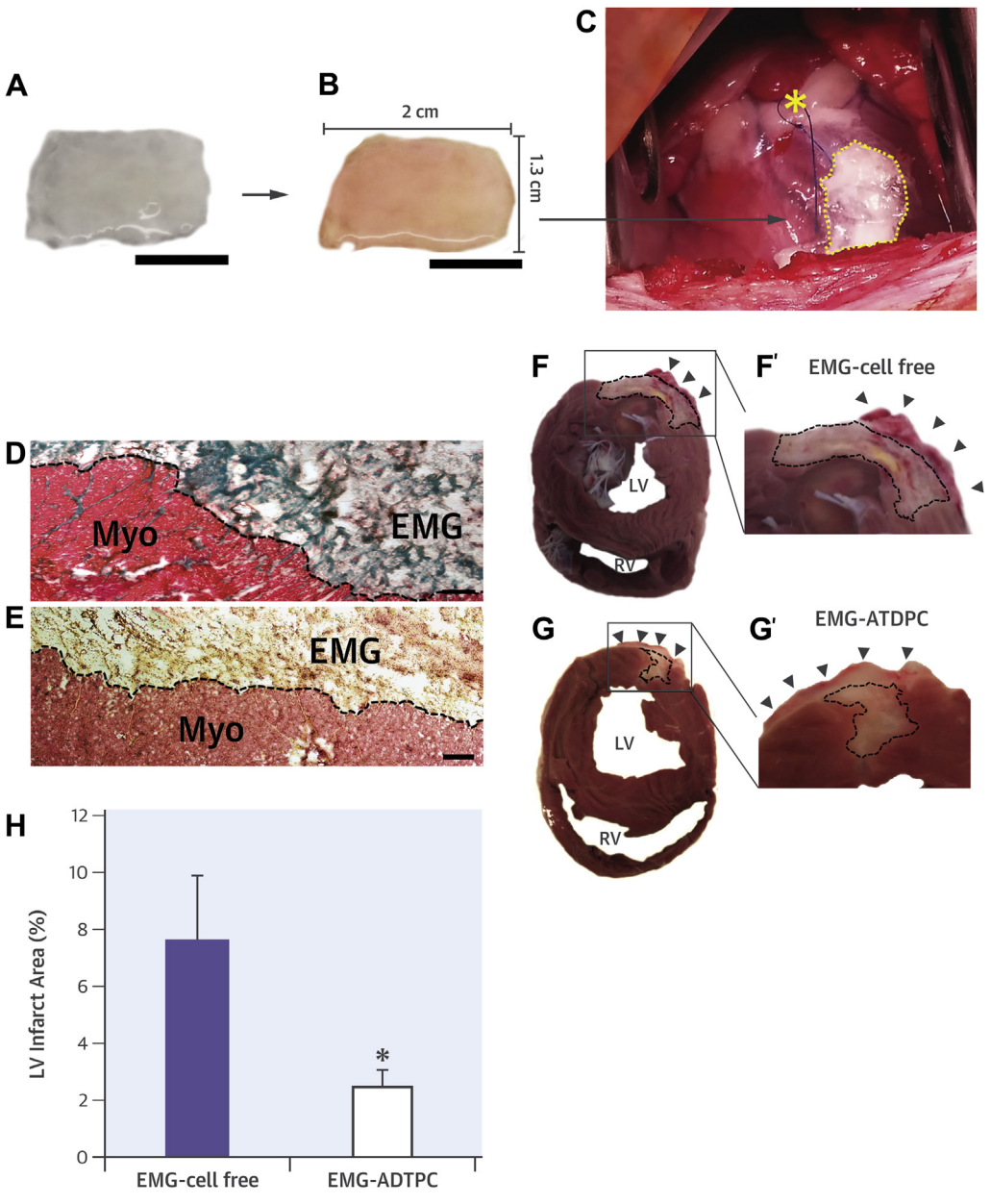

(A) The myocardial scaffold was embedded with the mixture of hydrogel and GFP^{+} pATDPCs. **(B)** Then culture medium was added, to facilitate hydrogel gelification and to generate the definitive EMG-ATDPC. Scale bars = 1 cm. **(C)** EMG-ATDPC (surrounded by a **dotted yellow line**) engrafted in the porcine heart over the MI performed by a coronary artery ligation (indicated with a **yellow asterisk**). **(D)** Panoramic micro-photograph of the implanted EMG-ATDPC over the myocardium, with histological assessment under Masson's trichrome and **(E)** Movat's pentrachrome stains. Scale bars = 100 μm. **(F)** Representative images showing the intact EMG **(black arrowheads)** retained over the infarcted myocardium **(discontinuous black line)** after animal sacrifice in EMG-cell free and **(G)** EMG-ATDPC pigs. **(F′)** Magnification of the infarcted area and EMG in the EMG-cell free and **(G′)** EMG-ATDPC groups, respectively. **(H)** Percentage of LV infarct area measured in the EMG-ATDPC and EMG-cell free groups. Data are expressed as mean ± SEM. *p = 0.048. GFP = green fluorescent protein; LV = left ventricle; Myo = host myocardium; RV = right ventricle; other abbreviations as in Figure 1.

3. EMG-sham (n = 2), with no MI and EMG-ATDPC over healthy myocardium.

Acute MI was induced by performing a left lateral thoracotomy, followed by permanent double ligation of the first marginal branch of the circumflex artery, as previously described (15). Thirty minutes later, the EMG-ATDPC or EMG-cell free was attached over the infarcted area using surgical glue (Glubran2, Cardiolink, Barcelona, Spain) (**Figure 2C**). To ensure induction of similar MI, blood samples were collected from all animals through jugular venipuncture at baseline and 2 h post-MI. The circulating cardiac biomarkers cardiac troponin I (cTnI) and creatinine kinase were measured using a fluorometric immunoassay analyzer (AQT90 FLEX, Radiometer Medical, Brønshøj, Denmark). Following completion of these procedures, the animals were housed for 1 month before sacrifice.

CARDIAC FUNCTION EVALUATION. Investigators blinded to treatment groups assessed the animals' cardiac function using cardiac magnetic resonance imaging (CMR) at 1.5-T (Intera, Philips, Amsterdam, the Netherlands) with a 4-channel, phased array surface coil (SENSE Body Coil). Acquired images were taken in apnea with electrocardiogram gating. At 3 time points—baseline, 48 h post-MI, and 1 month after treatment—we analyzed the following cardiac parameters: cardiac output, end-diastolic wall mass, left ventricular end-diastolic volume, left ventricular ejection fraction (LVEF), left ventricular end-systolic volume, and stroke volume.

HISTOPATHOLOGICAL EXAMINATION. Animals were sacrificed by administering an anesthesia overdose at 33.4 ± 4.2 days after the initial MI induction. Porcine hearts were then excised and sectioned. Extracted biopsies were embedded in Tissue O.C.T. compound (VWR Chemicals, Radnor, Pennsylvania), snap-frozen in liquid nitrogen, and then properly stored until analysis.

For morphometric quantitation of infarct size, the left ventricular (LV) infarct area was measured in photographed heart sections, 1.5 cm distally to the coronary ligation. Quantification was performed using Image J software (version 1.48, National Institutes of Health, Bethesda, Maryland). Infarct size was double-blindly measured by 2 independent investigators and calculated as the percentage of the LV infarct area relative to the LV total area.

Histological analyses of 10-μm frozen sections were performed with hematoxylin/eosin, Masson's trichrome, and Movat's pentachrome stains. We also used picrosirius red staining for scar fibrosis analysis to examine collagen deposition and changes in the amounts of type I and III collagens. Total collagen and specific I and III types were quantified for 6 random fields using Image-Pro Plus software (version 6.2.1, Media Cybernetics, Rockville, Maryland).

For detailed information about immunohistological analysis, see the Supplemental Appendix.

STATISTICAL ANALYSIS. Statistical analyses were performed using the statistics program SPSS (version 20, IBM, Armonk, New York). Both cardiac function differences and quantitative histopathological evaluation between groups were compared using the Student *t* test for paired and independent samples. Baseline CMR parameters differences were assessed with an analysis of variance test. Data are represented as mean ± SEM, and a p value <0.05 was considered statistically significant.

RESULTS

Following MI induction, 1 animal died due to ventricular fibrillation, 1 exhibited no evidence of MI and was thus not considered in the final analysis, and 2 animals were excluded due to post-surgical infection associated with inappropriate EMG handling during the preparation process before implantation. Thus, a total of 16 animals were finally included in the analysis (cardiac function and histopathology), distributed as follows: 7 in the EMG-cell free group, 7 in the EMG-ATDPC, and 2 in the EMG-sham group (**Figure 1**). The EMG-cell free and EMG-ATDPC groups showed similar levels of the circulating cardiac markers cTnI (0.06 ± 0.02 μg/l vs. 0.03 ± 0.05 μg/l; p = 0.55) and creatinine kinase MB (0.66 ± 0.29 μg/l vs. 0.43 ± 0.19 μg/l; p = 0.52), indicating similar MI induction in both groups. After macroscopic and microscopic examination, in 10 animals of 16 (n = 6 and n = 4 for EMG-cell free and EMG-ATDPC groups, respectively), the EMG remained properly attached to the underlying myocardium and was identifiable at both levels after 1 month (**Figures 2D to 2G′**). In the remaining animals, the EMG was reabsorbed and could not be distinguished following sacrifice.

EMG-ATDPC IMPLANTATION REDUCED INFARCT SIZE AND IMPROVED CARDIAC FUNCTION. LV infarct size was 68% smaller in the EMG-ATDPC compared with the EMG-cell free group (2.5 ± 0.6% vs. 7.6 ± 2.3%, respectively; p = 0.048) (**Figure 2H**).

Baseline CMR data analysis showed no differences between the studied groups (Supplemental Table 1). Cardiac function assessed by LVEF at 1 month follow-up after infarction significantly improved in the EMG-ATDPC group (50.8 ± 2.6% vs. 61.3 ± 3.4%; p = 0.001) and remained nonsignificant in the EMG-cell free group (48.4 ± 3.0% vs. 52.9 ± 2.2%;

FIGURE 3 Cardiac Function Evaluation by CMR

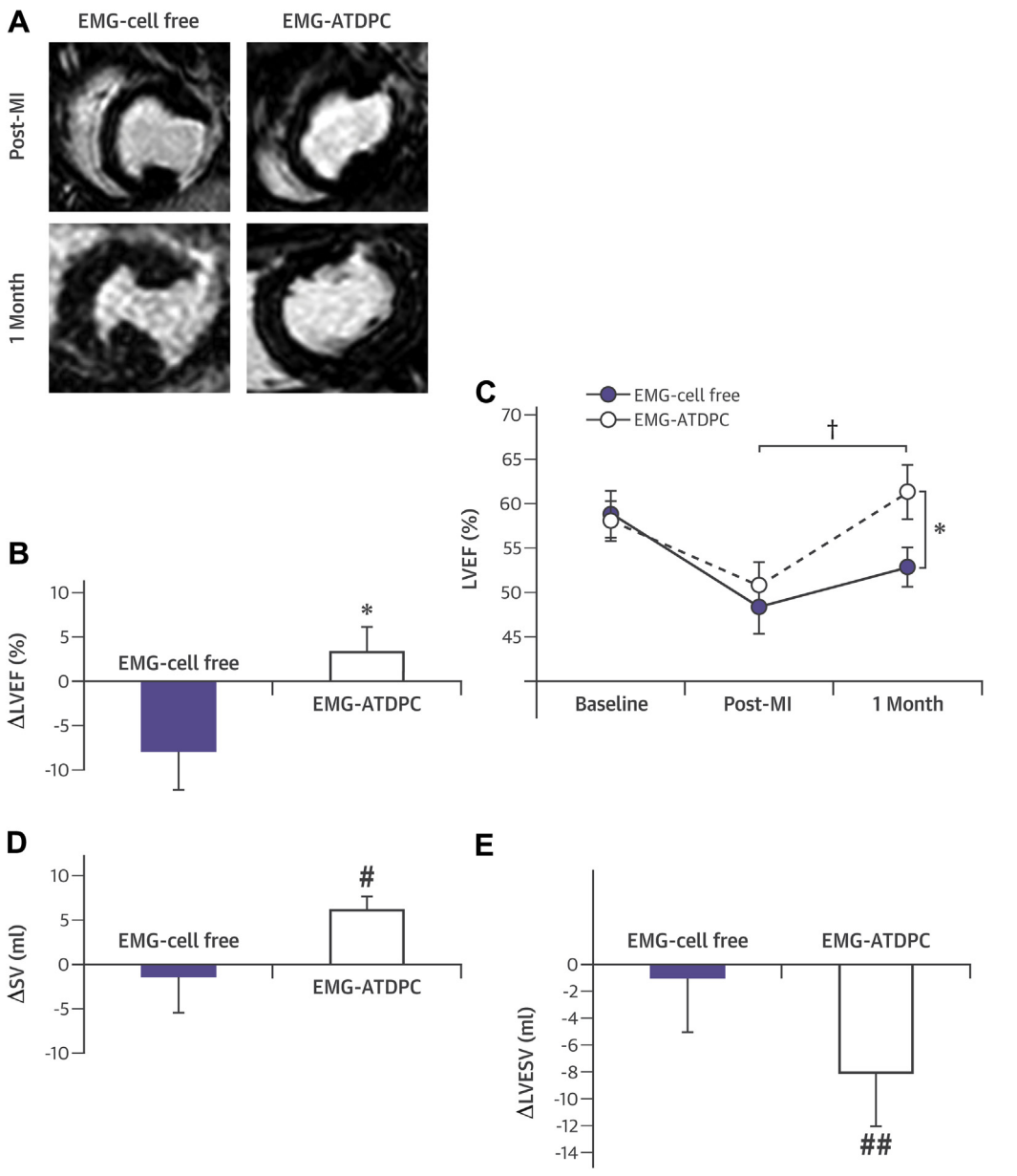

(A) T1 short-axis delayed enhancement images from EMG-cell free and EMG-ATDPC animals, at 48 h after MI induction **(upper panels)** and at 1 month, before sacrifice **(lower panels)**. **(B)** LVEF dynamics between baseline and 1 month for EMG-cell free and EMG-ATDPC groups, respectively. Data are shown as mean ± SEM. *p = 0.047. **(C)** LVEF for EMG-cell free and EMG-ATDPC groups at indicated time points: baseline, 48 h post-MI, and 1 month. Values are expressed as mean ± SEM. *p = 0.041, †p = 0.001. **(D)** SV differential values between baseline and 1 month for EMG-cell free and EMG-ATDPC groups. Data are represented as mean ± SEM. #p = 0.08 (trend). **(E)** LVESV differential measures between 48 h post-MI and after 1 month of follow-up for EMG-cell free and EMG-ATDPC animals. Data indicated as mean ± SEM. ##p = 0.09 (trend). CMR = cardiac magnetic resonance; LVEF = left ventricular ejection fraction; LVESV = left ventricular end-systolic volume; SV = stroke volume; other abbreviations as in Figure 1.

p = 0.30) (Figures 3A to 3C, Table 1). Similar trends were observed for stroke volume (6.1 ± 1.6 ml vs. −1.5 ± 4.0 ml, p = 0.08, for EMG-ATDPC vs. EMG-cell free, respectively) and LV end-systolic volume (−8.1 ± 1.4 ml vs. −1.0 ± 3.5 ml, p = 0.09, for EMG-ATDPC vs. EMG-cell free, respectively), indicating limited ventricular remodeling in treated animals (Figures 3D and 3E).

TABLE 1 CMR-Derived Cardiac Function Parameters

	EMG-Sham (n = 2)			EMG-Cell Free (n = 7)			EMG-ATDPC (n = 7)		
	48 h Post-Intervention	1 Month	p Value	48 h Post-MI	1 Month	p Value	48 h Post-MI	1 Month	p Value
CO (l/min)	2.9 ± 0.5	3.1 ± 0.5	0.76	3.1 ± 0.4	2.9 ± 0.1	0.41	2.9 ± 0.1	2.9 ± 0.2	0.95
EDWM (g)	66.9 ± 9.7	68.2 ± 5.6	0.81	69.9 ± 5.5	68.4 ± 4.7	0.60	69.0 ± 3.2	71.1 ± 3.5	0.42
LVEDV (ml)	61.5 ± 6.3	60.5 ± 10.0	0.83	64.7 ± 5.5	67.0 ± 5.1	0.63	66.2 ± 2.7	62.9 ± 2.6	0.21
LVEF (%)	54.4 ± 5.0	60.2 ± 0.3	0.44	48.4 ± 3.0	52.9 ± 2.2	0.30	50.8 ± 2.6	61.3 ± 3.1	**0.001**
LVESV (ml)	27.7 ± 0.2	24.1 ± 3.8	0.53	33.3 ± 3.3	32.3 ± 3.6	0.77	32.8 ± 2.5	24.7 ± 2.8	**0.001**
SV (ml)	33.8 ± 6.6	36.4 ± 6.2	0.08	31.4 ± 3.3	34.7 ± 1.9	0.34	33.5 ± 1.7	38.2 ± 1.1	**0.03**

Values are mean ± SEM. Cardiac function parameters in the EMG-sham, EMG-cell free, and EMG-ATDPC groups are at 48 h after MI induction (or post-intervention for EMG-sham) and at the time of sacrifice (1 month). The p values in **bold** are statistically significant.

ATDPC = adipose tissue-derived progenitor cells; CMR = cardiac magnetic resonance; CO = cardiac output; EDWM = end-diastolic wall mass; EMG = engineered myocardial graft; LVEDV = left ventricular end-diastolic volume; LVEF = left ventricular ejection fraction; LVESV = left ventricular end-systolic volume; MI = myocardial infarction; SV = stroke volume.

EMG-ATDPC PROMOTED NEOVASCULARIZATION OF SUBJACENT MYOCARDIUM AND INCREASED VESSEL DENSITY. EMG-ATDPC displayed notable vascularization, including formation of new vessels inside the construct (Figures 4A and 4B), with presence of erythrocytes and polymorphonuclear cells within, confirming functional conduits with blood flow (Figure 4C). These vessels showed positive staining for smooth muscle actin (SMA) in the tunica media (Figure 4D) and for CD31 and isolectin B4 (IsoB4) in the endothelial layer comprising the tunica intima (Figures 4E and 4F). Interestingly, some of the newly formed vessels connected the EMG-ATDPC with the underlying myocardium (Figures 4G to 4I), confirming its integration with the vascular network of the host myocardium. Moreover, vessel quantification revealed 2-fold higher vessel area in the EMG-ATDPC animals than in the EMG-cell free animals, both in the infarct core (3.6 ± 0.5% vs. 1.7 ± 0.1%; $p = 0.011$) and within the EMG (3.3 ± 0.3% vs. 1.5 ± 0.2%; $p < 0.001$) (Figure 4J).

GFP$^+$ pATDPCs MIGRATED TO THE HOST MYOCARDIUM AND EXPRESSED ENDOTHELIAL MARKERS. Histological analysis of the EMG-ATDPC explanted hearts revealed GFP$^+$ pATDPCs within the EMG (Figure 5A), as well as cell migration to the underlying infarct core (Figure 5B). Implanted cells were positive for SMA, maintaining its baseline expression, and remarkably, de novo expressed CD31 and IsoB4 (Figures 5C to 5E, Supplemental Figure 1). Altogether, this suggests that the introduced cell lineage contributed to the generation of new vessels and increased vascularization. These results also provided evidence of the commitment of pATDPCs toward an endothelial differentiation phenotype.

Evaluation of cell proliferative status in the infarct core revealed that GFP$^+$ pATDPCs exhibited nuclear co-staining with phospho-histone H3, a marker of active proliferation (data not shown). The total phospho-histone H3-positive cell count in the infarct core was almost 2-fold higher in the EMG-ATDPC group compared with the EMG-cell free group (1.5 ± 0.2% vs. 0.8 ± 0.2%, respectively; $p = 0.019$) (Supplemental Figure 2).

TREATMENT WITH EMG-ATDPC ATTENUATED MYOCARDIAL FIBROSIS FOLLOWING MI. We further examined the collagen content in the myocardial scar following MI induction to assess how the EMG engraftment affected fibrosis progression (Figures 6A to 6D). Focusing on the infarct area, total collagen content was significantly reduced in the EMG-ATDPC group compared to the EMG-cell free group (28.6 ± 6.1% vs. 49.9 ± 4.1%, respectively; $p = 0.016$). Collagen fibril subtype analysis revealed reduced type I collagen (19.8 ± 4.6% vs. 46.3 ± 4.4%; $p = 0.002$) and increased type III collagen (8.8 ± 2.0% vs. 3.6 ± 1.1%; $p = 0.042$) in EMG-ATDPC-treated animals. Hence, the ratio of type I to III was also significantly lower in EMG-ATDPC animals (2.3 ± 0.7 vs. 13.0 ± 6.9; $p = 0.032$) (Figure 6E).

DISCUSSION

The present study is the first, to our knowledge, to test an EMG comprising a decellularized myocardial scaffold plus adipose-derived progenitors (EMG-ATDPC) in a pre-clinical MI model. Herein, we investigated the functional benefits derived from EMG-ATDPC engraftment in terms of cardiac function, neovascularization, and scar healing. EMG-ATDPC treatment led to improved contractility (assessed by surrogate LVEF), 2-fold higher vascular density in the infarct area, 3-fold smaller infarct size, and modulation of scar healing with attenuated ventricular remodeling.

The pATDPC lineage chosen to repopulate the scaffold has previously exhibited cardiomyogenic

FIGURE 4 **Analysis of Post-MI Vascularization After EMG-ATDPC Engraftment**

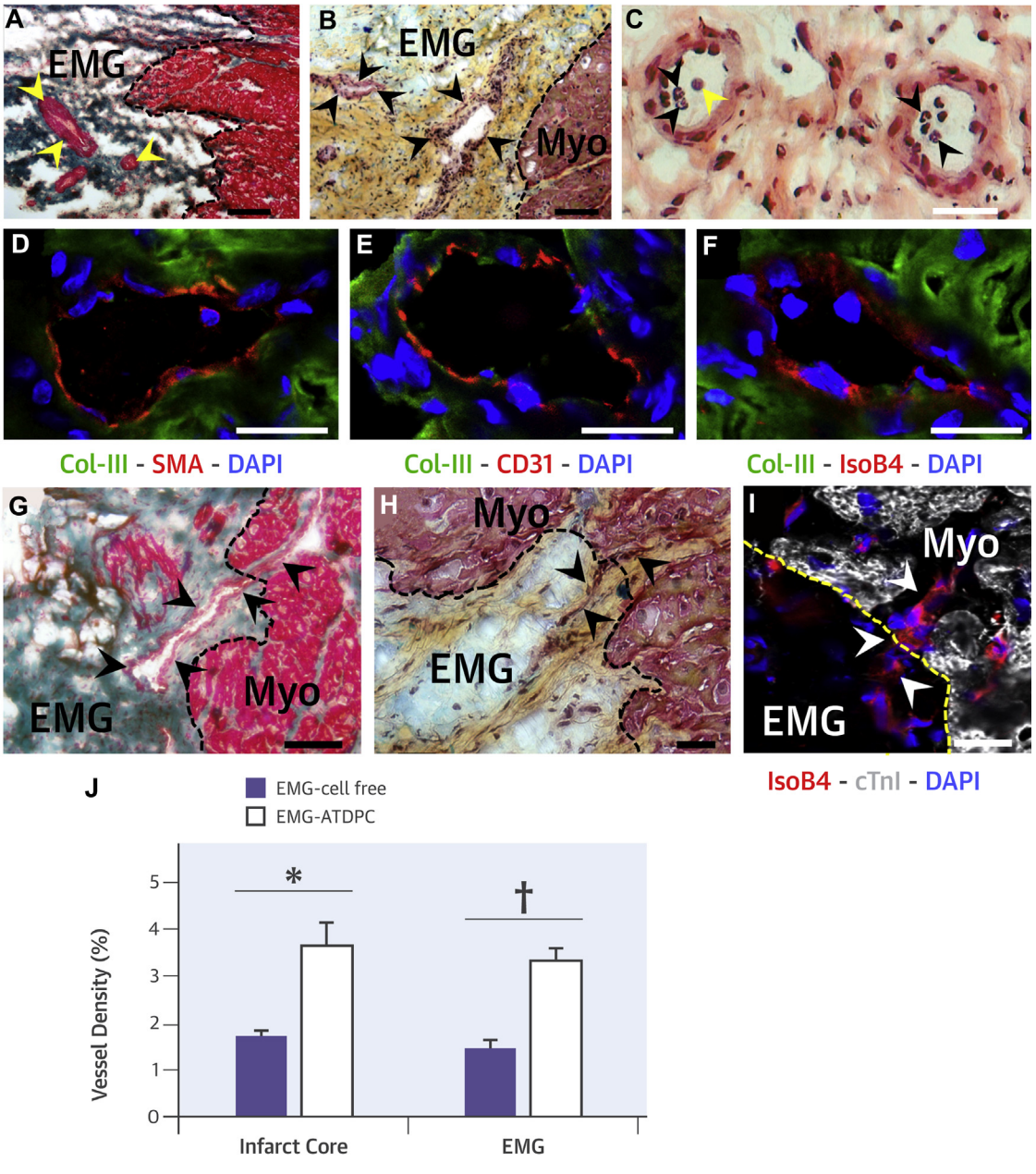

(A) Masson's trichrome and **(B)** Movat's pentachrome stains reveal presence of blood vessels in the EMG-ATDPC (**yellow and black arrowheads**, respectively). Scale bars = 100 and 50 μm, in that order. **(C)** Hematoxylin/eosin staining showing functional blood vessels in EMG-ATDPC with presence of polymorphonuclear cells **(black arrowheads)** and erythrocytes **(yellow arrowheads)** in the lumen. Scale bar = 20 μm. **(D)** Images of the EMG-ATDPC with immunohistochemistry revealing neovessels positive for SMA, **(E)** CD31, and **(F)** IsoB4 (**red** for all cases). Type III collagen (Col-III) was stained in **green**, and nuclei were counterstained with DAPI **(blue)**. Scale bars = 20 μm. **(G)** Neovessels connecting the engrafted EMG-ATDPC with the host myocardium **(arrowheads)** revealed with Masson's trichrome, **(H)** Movat's pentachrome, and **(I)** immunohistochemical staining (**red** indicates IsoB4; **grey**, cTnI; **blue**, nuclei). Scale bars = 50 μm **(G and H)** and 20 μm **(I)**. All images shown belong to the EMG-ATDPC animal group. **(J)** Percentage of vascular density in the infarct core and inside the EMG in the EMG-cell free and EMG-ATDPC groups. Final data are shown as mean ± SEM. *p = 0.011, †p < 0.001. cTnI = cardiac troponin I; IsoB4 = isolectin B4; SMA = smooth muscle actin; other abbreviations as in Figures 1 and 2.

FIGURE 5 Assessment of GFP$^+$ pATDPC Migration and Endothelial Differentiation in EMG-ATDPC Animals

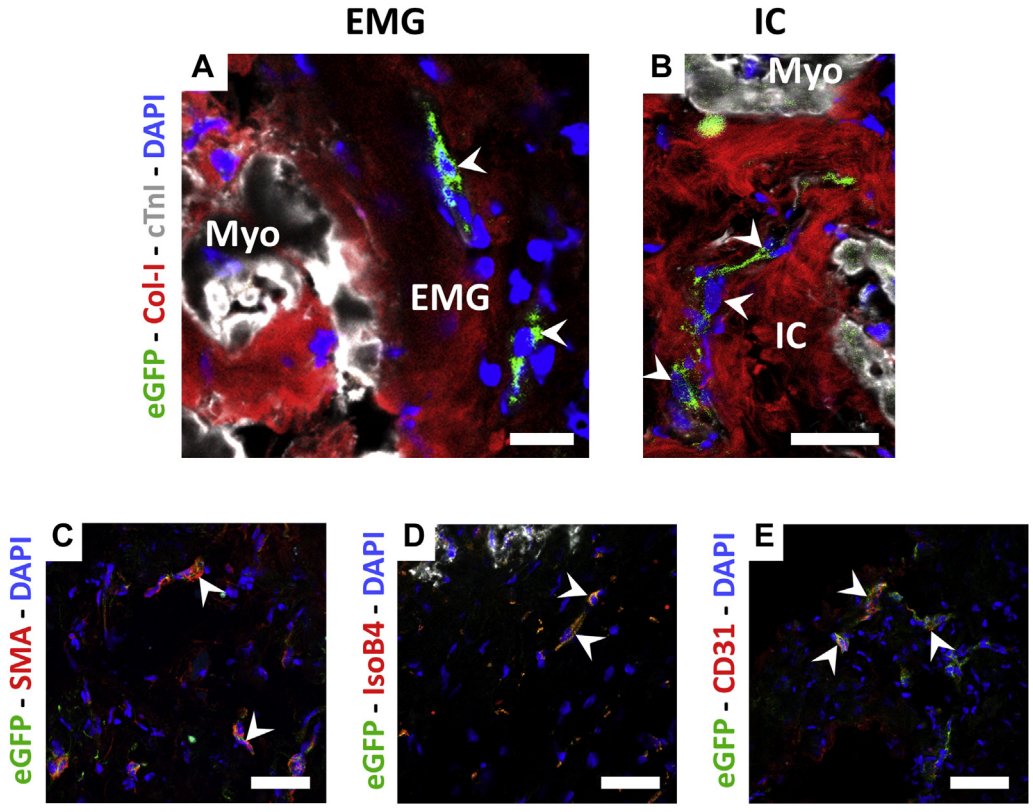

(A) Presence of GFP$^+$ pATDPCs **(green, white arrowheads)** in the EMG and **(B)** within the infarct core. Cardiomyocytes were labeled with cTnI **(grey)**, myocardial matrix fibers with type I collagen (Col-I, **red**), and nuclei were counterstained with DAPI **(blue)**. **(C)** Photographs of the infarct core of the EMG-ATDPC group with immunostaining for the endothelial markers SMA, **(D)** IsoB4, and **(E)** CD31 (**red** for all cases). Nuclei were counterstained with DAPI **(blue)** and **white arrowheads** indicate the GFP$^+$ pATDPCs **(green)** expressing the protein of interest. Scale bars = 20 μm. IC = infarct core; other abbreviations as in Figures 1, 2 and 4.

commitment and regenerative potential appropriate for cardiac tissue engineering (9,14,16). Moreover, their inherent immunomodulatory capacity facilitates delivery, eliminating the need for immunosuppressive treatments in the context of allogeneic transplantation (17,18). In vivo studies have also demonstrated that ATDPC delivery within scaffolds of diverse origin promotes remarkable cardiac function improvement in mice (19), rat (20,21), and porcine (14,22) MI models, supporting their suitability for in vivo application.

To better understand the beneficial effects exerted by the EMG-ATDPC, we must examine the synergistic contributions from the decellularized myocardial scaffold and the pATDPCs. The decellularized myocardial scaffold must preserve the native myocardial matrix integrity and organization, such that it can provide adequate cues to drive cell differentiation and to ensure cell attachment, survival, and migration (23,24). We must also acknowledge the role of the decellularized scaffolds themselves, in terms of neovascularization and cell recruitment. Engraftment of an acellular pericardial scaffold over porcine infarcted myocardium can reportedly prompt scaffold neoinnervation and neovascularization (25). Decellularized myocardial scaffolds apparently attract endogenous endothelial and smooth muscle cells, increasing vascular sprouting (26), and enabling scaffold-host tissue connections with vascular networks and irrigation of injured tissue. Thus, the decellularized myocardial scaffold both provides cellular supportive function and participates in direct vascularization of ischemic myocardium. Likewise, its porcine origin is advantageous for 2 main reasons: first, decellularized scaffolds can be easily obtained from pig hearts, with high

FIGURE 6 **Determination of Collagen Content and Composition in the Infarct Core**

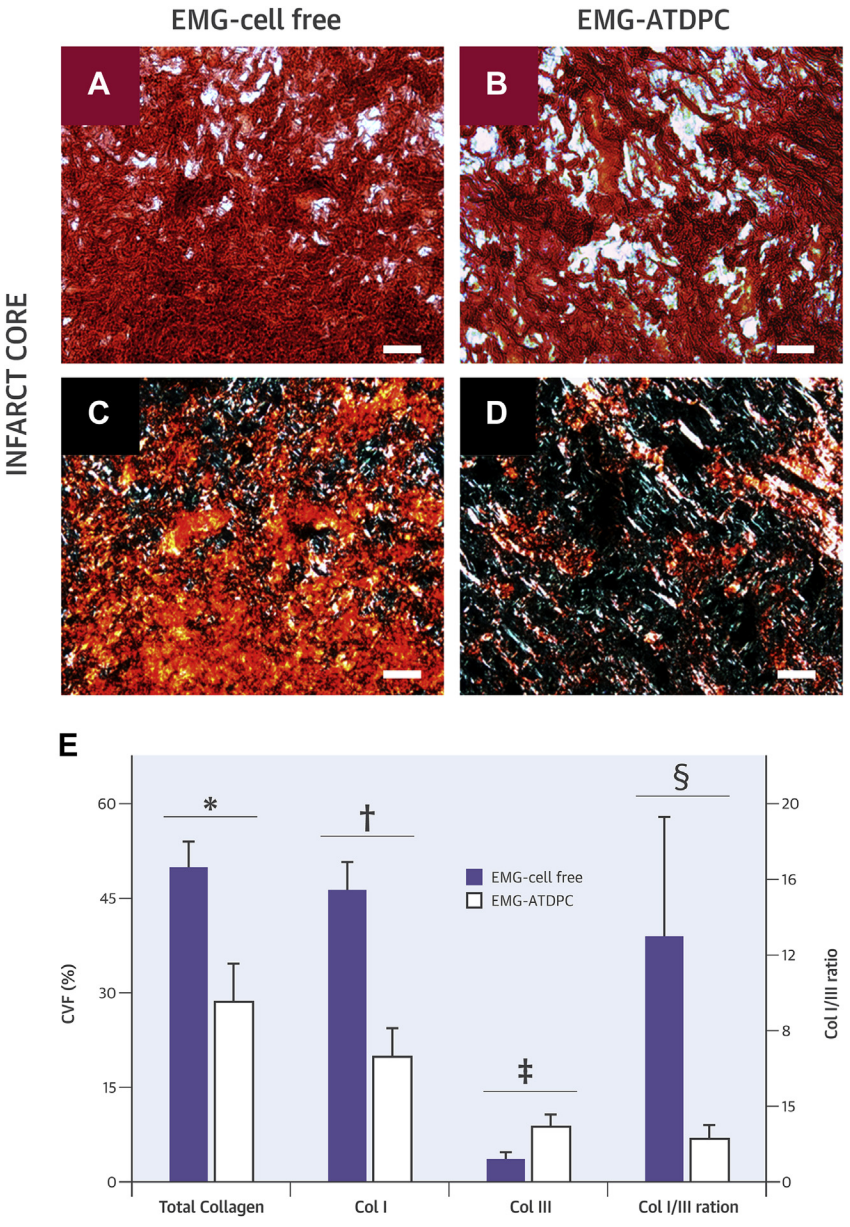

(A and B) Representative bright light microscopy images with sirius red staining distinguishing collagen fibers **(red)** and healthy myocardium **(yellow/orange)** from EMG-cell free and EMG-ATDPC animals, respectively. **(C and D)** Polarized light microscopy images with sirius red staining showing type I collagen **(red/yellow)** and type-III collagen **(green)** in the EMG-cell free and EMG-ATDPC groups, respectively. Scale bars = 50 μm. **(E)** Collagen percentage—expressed as collagen volume fraction (CVF [%], left y-axis)—for total collagen, type I collagen (Col I), and type III collagen (Col III); as well as the ratio between type I and III collagens (Col I/III ratio, right y-axis), for both the EMG-cell free and EMG-ATDPC groups. Results are displayed as mean ± SEM. *p = 0.016, †p = 0.002, ‡p = 0.042, §p = 0.032. Abbreviations as in Figure 1.

availability, and generated in large quantities; and second, some studies demonstrated feasible and viable administration in clinical practice of decellularized non-glutaraldehyde fixed xenograft with no associated side effects, immunological response, or rejection (27), overcoming fixation of porcine heart valves before implantation in humans to reduce immunogenicity and strengthen the tissue, but which in turn would impede cell repopulation and in some cases has led to calcification (28). Hence, clinical translation of this xenograft should not be hampered by regulatory issues.

On the other hand, the contribution of pATDPCs to infarct repair is likely even more important, and may be the key to understand post-MI recovery. The GFP^+ pATDPCs that migrated to the infarct core were positive for the endothelial markers SMA, IsoB4, and CD31. Thus, cell delivery within the EMG contributed to new blood vessel synthesis, as was previously reported (14). This explains the higher vascular density observed in EMG-ATDPC animals—which increases the supplies of nutrients, oxygen, and endogenous stem cells to the hypoxic area, probably preventing infarct expansion due to EMG-ATDPC implantation effect.

Most likely, paracrine effects would be the most plausible mechanism by which pATDPCs exerted their beneficial effects, which has been broadly described as one of the putative mechanisms for implanted cells to regenerate the scarred area (29,30). Once placed on top of the infarcted myocardium, the pATDPCs can also exert autocrine and paracrine effects. They secrete growth factors—such as vascular endothelial, fibroblast, hepatocyte and insulin growth factors, and transforming growth factor-β—which increase the vasculogenic, antiapoptotic/cardioprotective, and proliferative activities, as well as the recruitment of endogenous stem cells (31,32). It is also reported pATDPCs secrete interleukin-6, -7, -8, and -11, which act as phagocyte chemoattractants to eliminate cell debris and encourage cellular turnover and regeneration (31). Such actions are consistent with the reduced infarct size and enhanced vascular density observed after EMG-ATDPC treatment, as well as the higher cell proliferation displayed in the EMG-ATDPC group. Moreover, collagen content reduction may be correlated with the secretion of metalloproteinases by pATDPCs, which inhibits collagen synthesis, as it has been described for mesenchymal stem cells (33). However, there is no clear explanation for the increase in type III collagen. One possibility is that synthesis of type III collagen increases when pATDPCs are under mechanical stress or inside a 3-dimensional scaffold (34). The mechanical stimuli in the myocardium and the scaffold environment could have up-regulated pATDPCs type III collagen production, compensating for its degradation.

Along with the altered collagen content, we observed a decrease in the ratio of type I to type III collagen, indicating a reduction of collagen I deposition. Type III collagen is typically present during wound healing, and organizes to form an elastic fibrillar network, providing a framework to ensure correct alignment of type I collagen fibers and maintenance of normal heart shape and myocardium stiffness. On the other hand, type I collagen exhibits high stiffness, thus permitting chamber remodeling (35,36). Overall, the observed histopathological changes—including neovascularization, infarct area regeneration, and attenuation of fibrosis—globally enhanced cardiac function in terms of better LVEF, which is the most clinically relevant parameter for assessing heart function. Our results reflect an ~11% improvement in LVEF after MI in EMG-ATDPC group, which is higher than the 3% to 4% enhancement obtained with percutaneous coronary intervention (37), the 4% registered with bone marrow cell therapies (38), or the improvements obtained with other scaffolds in the swine MI model (13,39,40).

The reported feasibility and functional potential of catheter delivery of a decellularized myocardial scaffold in vivo (26) encouraged previous studies to use such scaffolds in pre-clinical models, although earlier studies showed little or modest benefits. Initial studies in the rat MI model produced controversial results regarding LVEF. Although Singelyn et al. (41) did not observe LVEF changes following decellularized myocardial scaffold administration, Dai et al. (42) reported a 4.3% increase in LVEF with scaffold treatment compared with controls. Neither study described higher neovascularization or altered final infarct size after scaffold treatment, nor examined collagen content modifications (41,42). Another study in rats investigated the addition of mesenchymal progenitor cells into a decellularized myocardial-fibrin composite scaffold, and reported increased angiogenesis, but did not assess LVEF, infarct size, or collagen variations (43). Finally, a prior work conducted in swine reported that administration of cell-free decellularized myocardial scaffold did not significantly affect LVEF when comparing post-MI and final LVEF values (13), in contrast to our presently remarkable LVEF increase in EMG-ATDPC-treated swine.

STUDY LIMITATIONS. One of the limitations in the present study is the lack of a MI-only control group, with no EMG-cell free or EMG-ATDPC implantation.

Although the data provided here by themselves indicate a meaningful improvement in cardiac function and myocardial restoration in EMG-ATDPC-treated animals, further studies including a MI-only group may help in elucidating the role of the decellularized myocardial scaffold and its beneficial effects over infarcted myocardium by itself.

Thus, the promising data reported here support proceeding to clinical translation. Our group has already started EMG-ATDPC production under good manufacturing practice conditions and has initiated the road to obtain approval by local regulators as first steps for a phase I clinical trial.

CONCLUSIONS

To summarize, we generated an EMG-ATDPC comprising a decellularized myocardial scaffold that was repopulated with pATDPCs. This EMG-ATDPC was implanted in a swine MI model, and cardiac recovery was assessed by CMR. The engrafted EMG-ATDPC promoted revascularization of the damaged tissue, reduced infarct size, attenuated ventricular remodeling and fibrosis progression, and improved cardiac function. This EMG-ATDPC is ready for clinical translation.

ACKNOWLEDGMENTS The authors thank L. Hernández, B. Fernández, and J. Maestre for technical assistance with animal surgeries and magnetic resonance imaging analysis.

REPRINT REQUESTS AND CORRESPONDENCE: Dr. Antoni Bayes-Genis, Head of Cardiology Service, Germans Trias i Pujol University Hospital, Crta. Canyet, s/n, 08916 Badalona, Barcelona, Spain. E-mail: abayesgenis@gmail.com.

PERSPECTIVES

COMPETENCY IN MEDICAL KNOWLEDGE: MI remains a top-ranked cause of death worldwide. Local delivery of natural scaffolds repopulated with cardiac progenitor cells (EMG-ATDPC) is a feasible approach with beneficial impact in cardiac function recovery. In our hands, the engraftment of a cell-enriched engineered myocardial graft in the pre-clinical MI model in swine resulted in better left ventricular ejection fraction, higher vessel density and neovascularization, reduced infarct size by 68%, and limited fibrosis.

TRANSLATIONAL OUTLOOK: EMG-ATDPC implantation in the infarcted myocardium improves cardiac recovery in the porcine pre-clinical MI model. The design of a phase I to II clinical trial in humans is mandatory to confirm and validate safety and efficacy. Thus, the EMG-ATDPC is ready to start the translational avenue toward first-in-man clinical trials.

REFERENCES

1. World Health Organization. The Top 10 Causes of Death. Fact sheet N°310. Updated May 2014. Available at: http://www.who.int/mediacentre/factsheets/fs310/en/. Accessed December 16, 2015.

2. Pfeffer MA, Braunwald E. Ventricular remodeling after myocardial infarction. Experimental observations and clinical implications. Circulation 1990;81:1161–72.

3. Bergmann O, Bhardwaj RD, Bernard S, et al. Evidence for cardiomyocyte renewal in humans. Science 2009;324:98–102.

4. Mollova M, Bersell K, Walsh S, et al. Cardiomyocyte proliferation contributes to heart growth in young humans. Proc Natl Acad Sci U S A 2013;110:1446–51.

5. Langer R, Vacanti JP. Tissue engineering. Science 1993;260:920–6.

6. Hirt MN, Hansen A, Eschenhagen T. Cardiac tissue engineering: state of the art. Circ Res 2014;114:354–67.

7. Vunjak-Novakovic G, Lui KO, Tandon N, et al. Bioengineering heart muscle: a paradigm for regenerative medicine. Annu Rev Biomed Eng 2011;13:245–67.

8. Radisic M, Park H, Gerecht S, et al. Biomimetic approach to cardiac tissue engineering. Philos Trans R Soc Lond B Biol Sci 2007;362:1357–68.

9. Perea-Gil I, Uriarte JJ, Prat-Vidal C, et al. In vitro comparative study of two decellularization protocols in search of an optimal myocardial scaffold for recellularization. Am J Transl Res 2015;7:558–73.

10. Ott HC, Matthiesen TS, Goh SK, et al. Perfusion-decellularized matrix: using nature's platform to engineer a bioartificial heart. Nat Med 2008;14:213–21.

11. Crapo PM, Gilbert TW, Badylak SF. An overview of tissue and whole organ decellularization processes. Biomaterials 2011;32:3233–43.

12. Guyette JP, Charest J, Mills RW, et al. Bioengineering human myocardium on native extracellular matrix. Circ Res 2016;118:56–72.

13. Seif-Naraghi SB, Singelyn JM, Salvatore MA, et al. Safety and efficacy of an injectable extracellular matrix hydrogel for treating myocardial infarction. Sci Transl Med 2013;5:173ra25.

14. Prat-Vidal C, Gálvez-Montón C, Puig-Sanvicens V, et al. Online monitoring of myocardial bioprosthesis for cardiac repair. Int J Cardiol 2014;174:654–61.

15. Gálvez-Montón C, Prat-Vidal C, Roura S, et al. Transposition of a pericardial-derived vascular adipose flap for myocardial salvage after infarct. Cardiovasc Res 2011;91:659–67.

16. Bayes-Genis A, Gálvez-Montón C, Prat-Vidal C, et al. Cardiac adipose tissue: a new frontier for cardiac regeneration? Int J Cardiol 2013;167:22–5.

17. Perea-Gil I, Monguió-Tortajada M, Gálvez-Montón C, et al. Preclinical evaluation of the immunomodulatory properties of cardiac adipose tissue progenitor cells using umbilical cord blood mesenchymal stem cells: a direct comparative study. Biomed Res Int 2015;2015:439808.

18. Cho KS, Park HK, Park HY, et al. IFATS collection: immunomodulatory effects of adipose tissue-derived stem cells in an allergic rhinitis mouse model. Stem Cells 2009;27:259–65.

19. Bagó JR, Soler-Botija C, Casani L, et al. Bioluminescence imaging of cardiomyogenic and vascular differentiation of cardiac and subcutaneous adipose tissue-derived progenitor cells in fibrin patches in a myocardium infarct model. Int J Cardiol 2013;169:288–95.

20. Wang H, Shi J, Wang Y, et al. Promotion of cardiac differentiation of brown adipose derived stem cells by chitosan hydrogel for repair after myocardial infarction. Biomaterials 2014;35:3986–98.

21. Sun CK, Zhen YY, Leu S, et al. Direct implantation versus platelet-rich fibrin-embedded adipose-derived mesenchymal stem cells in treating rat acute myocardial infarction. Int J Cardiol 2014;173:410–23.

22. Araña M, Gavira JJ, Peña E, et al. Epicardial delivery of collagen patches with adipose-derived stem cells in rat and minipig models of chronic myocardial infarction. Biomaterials 2014;35:143–51.

23. Badylak SF, Taylor D, Uygun K. Whole-organ tissue engineering: decellularization and recellularization of three-dimensional matrix scaffolds. Annu Rev Biomed Eng 2011;13:27–53.

24. French KM, Boopathy AV, DeQuach JA, et al. A naturally derived cardiac extracellular matrix enhances cardiac progenitor cell behavior in vitro. Acta Biomater 2012;8:4357–64.

25. Gálvez-Montón C, Fernandez-Figueras MT, Martí M, et al. Neoinnervation and neovascularization of acellular pericardial-derived scaffolds in myocardial infarcts. Stem Cell Res Ther 2015;6:108.

26. Singelyn JM, DeQuach JA, Seif-Naraghi SB, et al. Naturally derived myocardial matrix as an injectable scaffold for cardiac tissue engineering. Biomaterials 2009;30:5409–16.

27. Konertz W, Angeli E, Tarusinov G, et al. Right ventricular outflow tract reconstruction with decellularized porcine xenografts in patients with congenital heart disease. J Heart Valve Dis 2011; 20:341–7.

28. Erdbrügger W, Konertz W, Dohmen P, et al. Decellularized xenogenic heart valves reveal remodeling and growth potential in vivo. Tissue Eng 2006;12:2059–68.

29. Doppler SA, Deutsch MA, Lange R, et al. Cardiac regeneration: current therapies-future concepts. J Thorac Dis 2013;5:683–97.

30. Hoke NN, Salloum FN, Loesser-Casey KE, et al. Cardiac regenerative potential of adipose tissue-derived stem cells. Acta Physiol Hung 2009;96: 251–65.

31. Gimble JM, Katz AJ, Bunnell BA. Adipose-derived stem cells for regenerative medicine. Circ Res 2007;100:1249–60.

32. Kokai LE, Marra K, Rubin JP. Adipose stem cells: biology and clinical applications for tissue repair and regeneration. Transl Res 2014;163:399–408.

33. Mias C, Lairez O, Trouche E, et al. Mesenchymal stem cells promote matrix metalloproteinase secretion by cardiac fibroblasts and reduce cardiac ventricular fibrosis after myocardial infarction. Stem Cells 2009;27:2734–43.

34. Colazzo F, Sarathchandra P, Smolenski RT, et al. Extracellular matrix production by adipose-derived stem cells: implications for heart valve tissue engineering. Biomaterials 2011;32:119–27.

35. Pauschinger M, Knopf D, Petschauer S, et al. Dilated cardiomyopathy is associated with significant changes in collagen type I/III ratio. Circulation 1999;99:2750–6.

36. Weber KT. Cardiac interstitium in health and disease: the fibrillar collagen network. J Am Coll Cardiol 1989;13:1637–52.

37. Strauer BE, Steinhoff G. 10 years of intracoronary and intramyocardial bone marrow stem cell therapy of the heart: from the methodological origin to clinical practice. J Am Coll Cardiol 2011; 58:1095–104.

38. Jeevanantham V, Butler M, Saad A, et al. Adult bone marrow cell therapy improves survival and induces long-term improvement in cardiac parameters: a systematic review and meta-analysis. Circulation 2012;126:551–68.

39. Mukherjee R, Zavadzkas JA, Saunders SM, et al. Targeted myocardial microinjections of a biocomposite material reduces infarct expansion in pigs. Ann Thorac Surg 2008;86: 1268–76.

40. Ye L, Chang YH, Xiong Q, et al. Cardiac repair in a porcine model of acute myocardial infarction with human induced pluripotent stem cell-derived cardiovascular cells. Cell Stem Cell 2014;15: 750–61.

41. Singelyn JM, Sundaramurthy P, Johnson TD, et al. Catheter-deliverable hydrogel derived from decellularized ventricular extracellular matrix increases endogenous cardiomyocytes and preserves cardiac function post-myocardial infarction. J Am Coll Cardiol 2012;59:751–63.

42. Dai W, Gerczuk P, Zhang Y, et al. Intramyocardial injection of heart tissue-derived extracellular matrix improves postinfarction cardiac function in rats. J Cardiovasc Pharmacol Ther 2013;18:270–9.

43. Godier-Furnémont AFG, Martens TP, Koeckert MS, et al. Composite scaffold provides a cell delivery platform for cardiovascular repair. Proc Natl Acad Sci U S A 2011;108:7974–9.

KEY WORDS adipose tissue-derived progenitor cells, cardiac tissue engineering, decellularized myocardial scaffold, myocardial infarction, pre-clinical model

APPENDIX For an expanded Methods section as well as a supplemental table and figures, please see the online version of this article.